Evolution of the central safety factor during stabilized sawtooth instabilities at KSTAR

PAPER

Evolution of the central safety factor during stabilized sawtooth instabilities at KSTAR

IOP Publishing | International Atomic Energy Agency Nuclear Fusion

Nucl. Fusion **58** (2018) 016030 (9pp) https://doi.org/10.1088/1741-4326/aa9484

Evolution of the central safety factor during stabilized sawtooth instabilities at KSTAR

M.C.C. Messmer[1], J. Ko[2,3], J. Chung[2], M.H. Woo[2], K.-D. Lee[2] and R.J.E. Jaspers[1,4]

[1] Eindhoven University of Technology (TU/e), 5600MB Eindhoven, Netherlands
[2] National Fusion Research Institute (NFRI), Daejeon 34133, Republic of Korea
[3] University of Science and Technology (UST), Daejeon 34113, Republic of Korea
[4] Department of Applied Physics, Ghent University, 9000 Ghent, Belgium

E-mail: m.c.c.messmer@tue.nl

Received 16 August 2017, revised 9 October 2017
Accepted for publication 19 October 2017
Published 16 November 2017

Abstract

A motional Stark effect (MSE) diagnostic has recently been installed in the KSTAR tokamak. A difficulty faced at KSTAR and common to other MSE diagnostics is calibration of the system for absolute measurements. In this report we present our novel calibration routine and discuss first results, evaluating the evolution of the the central safety factor during sawtooth instabilities. The calibration scheme ensures that the bandpass filters typically used in MSE systems are aligned correctly and identifies and removes systematic offsets present in the measurement. This is verified by comparing the reconstructed safety factor profile against various discharges where the locations of rational q surfaces have been obtained from MHD markers. The calibration is applied to analyse the evolution of q_0 in a shot where the sawteeth are stabilized by neutral beam injection. Within the analysed sawtooth periods q_0 drops below unity during the quiescent phase and relaxes close to or slightly above unity at the sawtooth crash. This finding is in line with the classical Kadomtsev model of full magnetic reconnection and earlier findings at JET.

Keywords: MSE, sawtooth, central safety factor, motional Stark effect, q_0, calibration

(Some figures may appear in colour only in the online journal)

1. Introduction

One of the outstanding challenges in tokamak research is the control of the current density profile for plasma control and its optimisation for high performance discharges. To resolve the internal magnetic field structure in a tokamak and reconstruct the current density profile, optical spectroscopy measuring the light emitted by fast neutral particles injected into the plasma is used. The technique proposed by Levinton [1] exploits the Stark effect and is dubbed the motional Stark effect (MSE) diagnostic. It enables a direct, local measurement of the magnetic pitch angle $\gamma_m(r) \equiv \tan^{-1}(B_\theta(r)/B_\phi(r))$, where B_θ and B_ϕ denote the poloidal and toroidal components of the magnetic field, respectively. From γ_m in combination with a Grad–Shafranov equation solvers, such as EFIT [2], the current density profile can be reconstructed. KSTAR recently showcased its capabilities by setting a new record for long pulse H-mode operation [3], however to support the ITER project in exploring advanced scenarios, current profile measurements are of essence. For this reason, a 25 chord MSE polarimeter has been installed in 2015 [4] and commissioned during the 2015 plasma campaign. Owing to the digital data acquisition system combined with digital lock-in analysis, the full Stokes vector is reconstructed on a millisecond timescale. From this the magnetic pitch angle can be calculated with a statistical uncertainty below 0.2° on 10 ms time averages, resulting in a accuracy of the safety factor at the magnetic axis of $\Delta q_0 \approx 0.1$ [5]. In this report, after giving an overview of the experimental setup at KSTAR, a generic two-step calibration and verification method is presented: First the bandpass filters used to single out the red-shifted Stark peak are calibrated such, that the measured pitch angle displays a physically reasonable slope. In the second step it is investigated whether systematic offsets are present by comparing the reconstructed q-profile

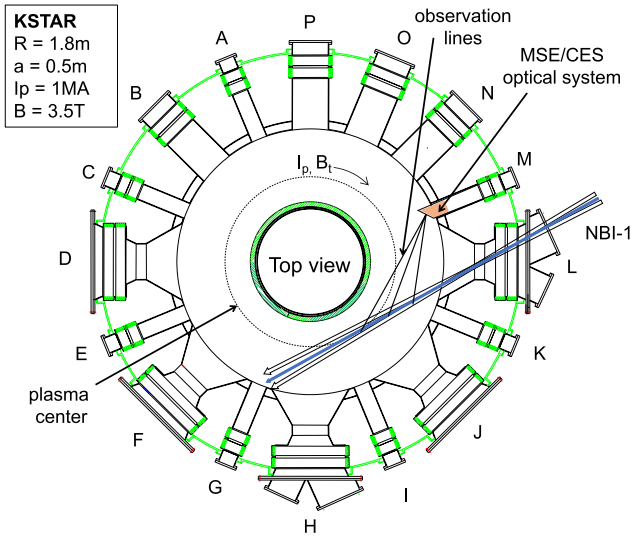

Figure 1. Equatorial cut of the KSTAR vessel including NBI-1 marked in blue and the MSE lines of sight. Adapted from [6], with the permission of AIP Publishing.

(constrained by MSE) against rational q-values obtainable from independent diagnostics during MHD instabilities in the plasma. After successful calibration, the q-profile evolution of a sawtooth crash is analysed in section 4.

2. Experimental setup

The MSE system at KSTAR has been installed prior to the 2015 plasma campaign during which it was commissioned. It measures the emission of high velocity neutral deuterium particles injected by one of KSTAR's neutral heating beams. A detailed report of the setup, including a description of the in-vessel calibration and correction of the Faraday rotation, can be found at [4, 6, 7]. A brief overview of the setup will be given for completeness. Figure 1 shows an equatorial cut of the tokamak torus and the three available heating beams. Due to the different injection angles and the induced Doppler shift, the Balmer-α emission of NBI-1 can be separated from the other beams and the background emission. The emitted light is captured by collection optics located in the M-port of the vessel. It is guided through two photoelastic modulators (PEM) oscillating at 23 kHz and 20 kHz and after passing through a linear polariser projected onto 25 fibre bundles. The resulting 25 radial channels span across the magnetic axis to the plasma edge, from $R = 1.74$ m to 2.28 m with a spacing of 2 cm.

Through the fibres, the light is transmitted to the optics laboratory for signal processing. It propagates through wavelength-tuneable 2 cavity Lorentzian shaped, 3 Å FWHM bandpass filter and is recorded by APD's with 2 MHz sampling rate. For the reconstruction of the Stokes vector and calculation of the magnetic pitch angle, the polarisation of the red-shifted π-peak is calculated. This line is chosen as it provides the lowest overlap with emission from the other neutral beams. The filters are initially rotated such that their central wavelength (CWL) matches the wavelength were we expect the highest emission intensity in the π spectrum, shown in figure 2. This position is forth on denoted as λ_0 or 0° offset.

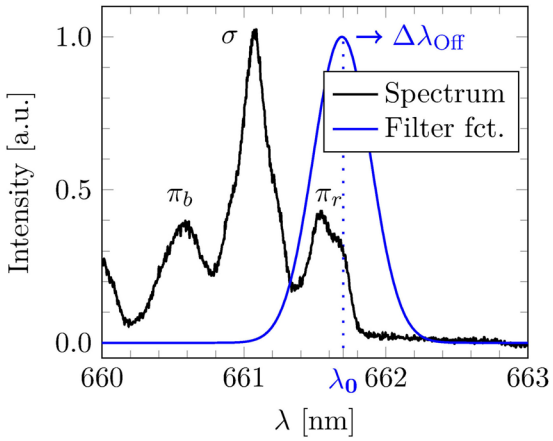

Figure 2. Recorded spectrum of shot *#12692*, channel 12 and filter function of the bandpass filter. In order to calibrate the bandpass filters, the CWL of the filters are stepwise red-shifted from their initial position λ_0 by increasing offsets $\Delta\lambda_{\text{Off}}$.

Deviations from λ_0 will be denoted as offsets $\Delta\lambda_{\text{Off}}$. First measurements showed that the initial filter position λ_0 was leading to unphysical results and thus a more elaborate calibration is required. The system is calibrated using a two-step approach: First, the optimal CWL of the bandpass filters is found, based on the linear polarisation fraction of the recorded signal (section 3.1) and second it is ensured that no systematic offsets are present in the recorded signal by cross-calibrating the reconstructed q-profile against independent diagnostics available at KSTAR (section 3.2).

3. Calibration of the MSE system

3.1. Alignment of the bandpass filters

Of crucial importance for the performance of the system is the correct alignment of the bandpass filters. From figure 2 one expects better signal-to-noise ratio by blue-shifting the filter function, but at the cost of signal quality as the recorded light will be contaminated by emission from the σ-peaks. To find the optimum filter position, four calibration shots with equal plasma equilibrium at a magnetic field strength $B_\phi = 2.9$ T and NBI acceleration voltage $U_{\text{NBI}} = 100$ keV were performed. In these L-mode discharges only NBI-1 beam was active and the CWL of the filter was incrementally red shifted between the shots. To increase the number of calibration points, the filter's CWL was additionally changed in the middle of each shot. Figure 3 shows the time evolution of the polarisation angle of shot *#13691*, where the filter position was shifted by $\Delta\lambda_{\text{Off}} = 1$ Å at $t \approx 4.5$ s. Although the plasma equilibrium did not change during the measurement, a clear shift in the recorded polarisation angle during the time of the filter rotation can be observed.

This behaviour has been observed for all channels throughout the calibration discharges. The effect on the radial profile is shown in figure 4, which displays the measured polarisation angle profile for shot *#13691* shortly before and after the filter was rotated. Aside the described shift in polarisation angle, the profiles show an oscillating pattern in the central and outer channels, whereas one would expect a smooth gradient from the nature of the plasma equilibrium.

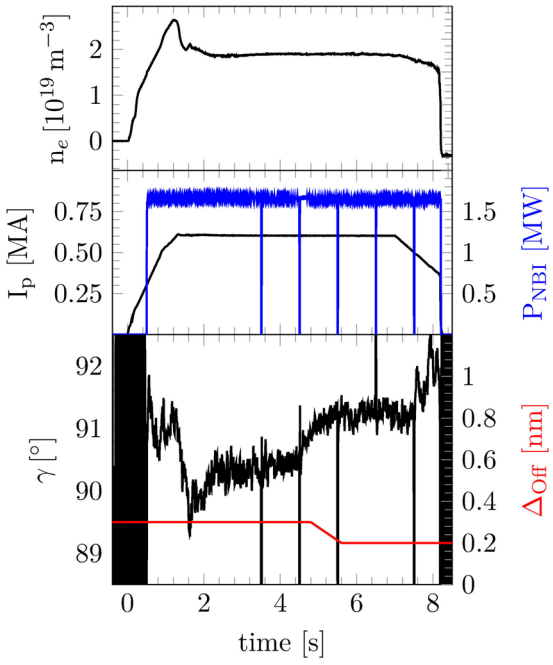

Figure 3. Time evolution of shot *#13691*. Top: line averaged density. Middle: Plasma current and injected NBI power. Bottom: polarisation angle and filter offset of channel 6. *Note:* The blips in the neutral beam are for charge exchange measurements.

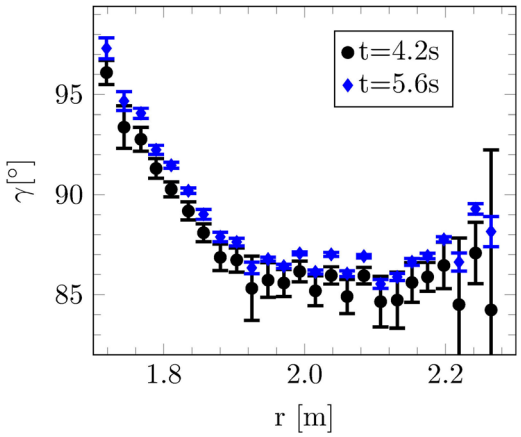

Figure 4. Radial polarisation angle profile of shot *#13691* before (4.2 s) and after (5.6 s) the filter rotation.

To calibrate the system, we make use of the digital data acquisition system, with which the full Stokes vector can be reconstructed. From this, the linear polarisation fraction (LPF) $\sqrt{S_1^2 + S_2^2}/S_0$, where the S_i are the ith component of the Stokes vector $S = (S_1, S_2, S_3, S_4)$, can be calculated. The LPF is evaluated for each offset $\Delta\lambda_{Off}$ and each channel. Figure 5 shows the LPF and total intensity over the filter offsets for channel 6[5].

[5] Alternatively it would be possible to use a non-MSE-constrained equilibrium solver to calculate the q-profile (and the magnetic pitch angle) for each shot and each time step and compare it to the measured magnetic pitch angle to find the optimum. However, since the q-profile obtained by an equilibrium solver such as EFIT without MSE is even in L-mode shots only an educated guess, a different method has been chosen.

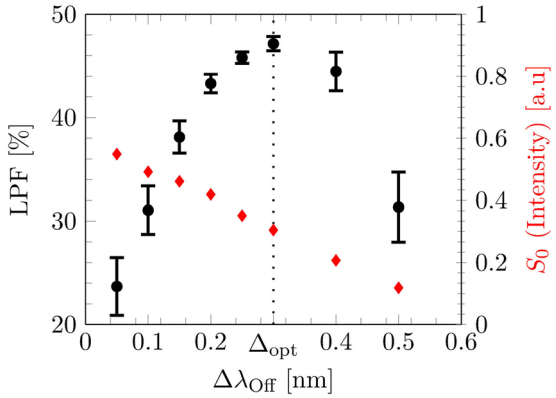

Figure 5. Linear polarisation fraction (circles) and total intensity S_0 (diamonds) of channel 6, shot *#13691* over $\Delta\lambda_{Off}$. The signals have been averaged over 300 ms.

As expected, the total intensity decreases by red-shifting the CWL of the filter. The LPF displays a quadratic dependence on the filter rotation (as it is expected from simulations [8]) and has its maximum, for channel 6, at $\Delta\lambda_{Off} \approx 0.3$ nm. A second order approximation is used to determine the optimum offset, defined as the position where the LPF has its maximum, for each channel. The obtained filter calibration was tested on two consecutive shots with identical plasma equilibrium. Here, the optimal filter settings were applied only to the later shot to see the effect of the calibration in comparison to the original filter settings, used at the first shot. Figure 6 compares the polarisation angle profile of the two at similar times of the discharge.

By optimising the filter rotation we almost completely eliminated the oscillations in the pitch angle profile. The measured radial profile has a continuous gradient and reduced uncertainties compared to the non-optimised discharge, giving confidence in the calibration method.

3.1.1. Post-shot calibration algorithm. The calibration of the filters was completed mid-campaign, which meant that roughly half of the campaign shots had been recorded using misaligned bandpass filters. To enable an analysis of these shots an algorithm has been developed to correct for the filter misalignment. The algorithm is illustrated in figure 7. The graph shows an analysis of the calibration shots similar to figure 5, but instead of plotting the dependency of the LPF on the filter rotation, the polarisation angles (averaged over the intervals of constant filter rotation) are plotted over the filter rotation. The graph shows a linear dependence of the polarisation angle over the offset, assuming that all shots have a similar plasma equilibrium over time. From physical intuition a flattening of the curve for higher values of $\Delta\lambda_{Off}$ is expected, once none of the light emitted by the σ-peaks overlaps with the envelope of the bandpass filters. However, this relationship can not be deduced from the recorded data due to the low signal strength and increasing uncertainties at big filter offsets.

To re-calibrate the polarisation angles of an incorrectly calibrated shot, the polarisation angle matching the determined ideal offset and the one matching the set offset of the shot are interpolated from the calibration curve in figure 7, marked

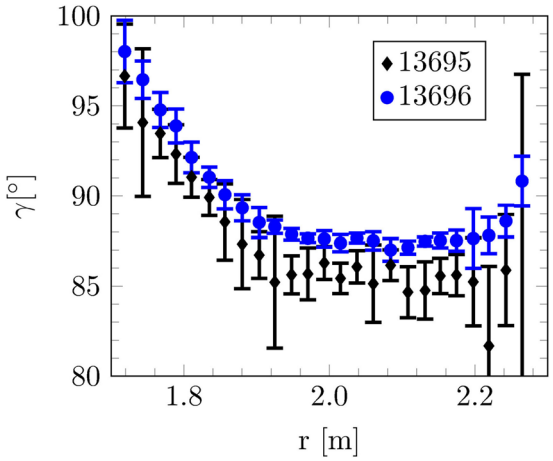

Figure 6. Polarisation angle profile for shots *#13695, #13696* at $t = 1.65$ s. The calculated, optimal filter settings have been applied to shot *#13696*, resulting in a smooth pitch angle profile with reduced uncertainties.

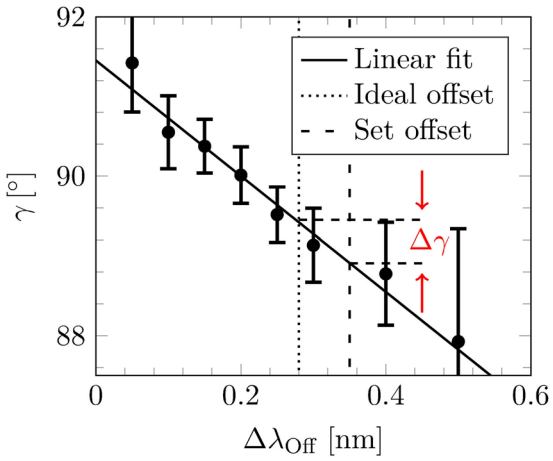

Figure 7. Dependence of the measured polarisation angle γ from channel 6 on the filter offsets in the calibration shots.

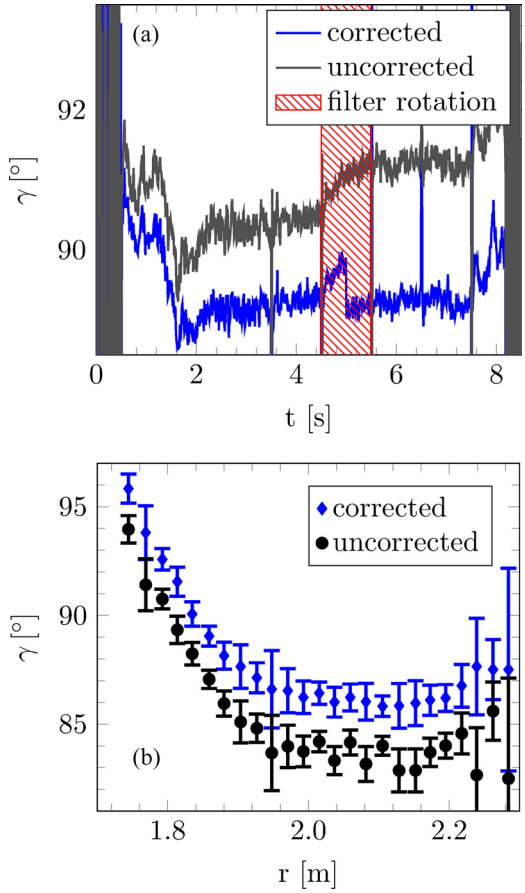

Figure 8. Post-shot filter correction for shot *#13691*. In the time evolution (*a*) the times during which the filter rotation was changed are shaded in red. In (*b*), the effect on the radial profile is shown. The uncorrected data has been shifted by $-2°$ for improved readability of the graph.

exemplary by the dotted and dashed line. The recorded polarisation angles of the discharge are then corrected by $\Delta\gamma$.

The correction algorithm is demonstrated on one of the four calibration shots in figure 8. The top figure shows the effect of the correction algorithm on the time evolution of γ. Here, the polarisation angle is now at a constant value before and after the change in filter rotation, lasting from $t \approx 4.4$ s –5.5 s, and lowered by approximately one degree. Note that the jump of the corrected polarisation angle at $t = 5$ s is due to the change in the correction factor $\Delta\gamma$. Because of the change in filter rotation, the set offset must be adapted in the algorithm, which has been done at an arbitrary time point during the filter rotation. The re-calibrated γ-profile is shown in figure 8(*b*). In contrast to the profile shown in figure 6, the uncertainty in the measurement is not reduced due to the interpolation mechanism.

3.2. Determination of systematic offset

After calibrating the bandpass filters to achieve physically sensitive measurements, the last step in the calibration procedure is to ensure that no systematic offsets are present in the recorded data. These could arise from an inaccurate determination of the measurement location in the vessel or from changes in the refractive index of the port window due to stress on the material induced from evacuating the vessel. To validate our measurements we compare the plasma equilibrium against tearing modes (TM) of known mode number and location. The plasma equilibrium is reconstructed with the Grad–Shafranov solver EFIT [2], which can be constrained by magnetic pitch angle measurements to reconstruct the current density profile. Initial attempts to reconstruct the MSE-constrained plasma equilibrium did not result in a converging solutions, which lead to the hypothesis of a systematic offset in the measurement. To determine the offset we repeatedly analysed the same shot with varying, channel independent offsets and compared the mode number and location of rational q-surfaces (determined by Mirnov Coils and ECE analysis) against the reconstructed equilibria. With this method a systematic offset of $-1.95°$ was found. A detailed description of the analysis is presented in appendix. This finding has been verified by evaluating the position of the magnetic axis (which can be determined directly from the pitch angles) against the axis position determined by magnetics only EFIT. The result,

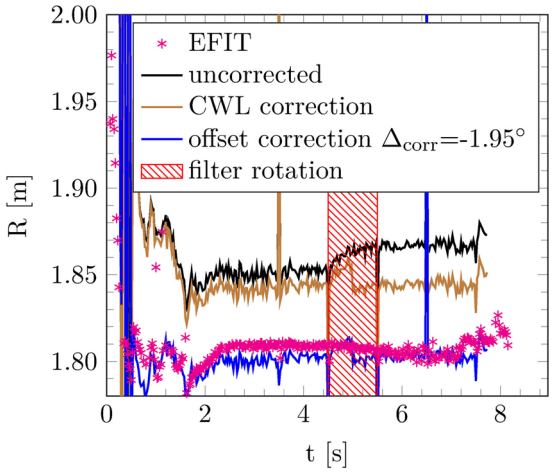

Figure 9. Comparison of the magnetic axis calculated from MSE measurements against the position obtained from magnetics only EFIT. The MSE measurements have been corrected by the post-shot filter rotation correction and the determined systematic offset of −1.95°.

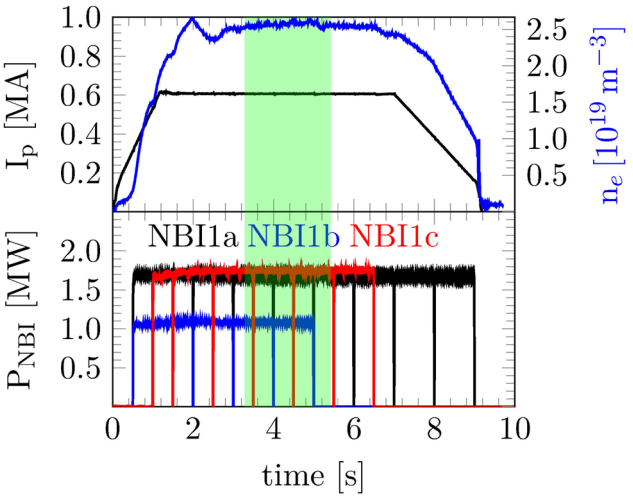

Figure 10. Time evolution of shot *#16499*. Top: Plasma current and line averaged density. Botton: NBI power. The sawtooth evaluation is limited to the area shaded in green.

shown in figure 9, shows good agreement between the magnetic axis location determined by EFIT (∗ ∗ ∗) and the axis position reconstructed from the polarisation angle measurements after the filter rotation correction and systematic offset correction have been applied (——). The full description of the analysis is included in appendix.

4. Evaluation of q_0 during sawtooth instabilities

After having successfully calibrated and verified the results obtained by the MSE diagnostic, the evolution of q_0 during sawtooth instabilities [9] is evaluated as a first application of the commissioned system. Despite tremendous effort, the underlying physics of the sawtooth instability have still not been fully understood and in the past 40+ years since its discovery various models have been proposed. Kadomtsev [10] explained the phenomena with full magnetic reconnection, however his model falls short of explaining the fast timescales of the sawtooth crash. Wesson [11] later suggested that a destabilising potential builds up during the ramp phase, which is released by a magnetic trigger and reconnection does not take place during the crash, but rather during the current ramp phase. Both models assume q_0 to rise to or above unity, however initial polarimetry measurements by Soltwisch [12] resulted in q_0 remaining well below unity on Textor. Measurements at TFTR [13] and JET [14] (and again Textor [15]) confirmed Soltwisch's findings. DIII-D initially reported similar results [16], but later claimed q_0 rising to unity after the sawtooth collapse [17].

Various other models have been proposed, however none was able to fully explain the measured observations. The presented analysis is focused on the investigation of the principal question, whether the evolution of the central safety factor evolves to or around unity during the sawtooth cycle. The short sawtooth period at KSTAR of typically 5 ms complicates spectroscopic analysis of the safety factor evolution, however

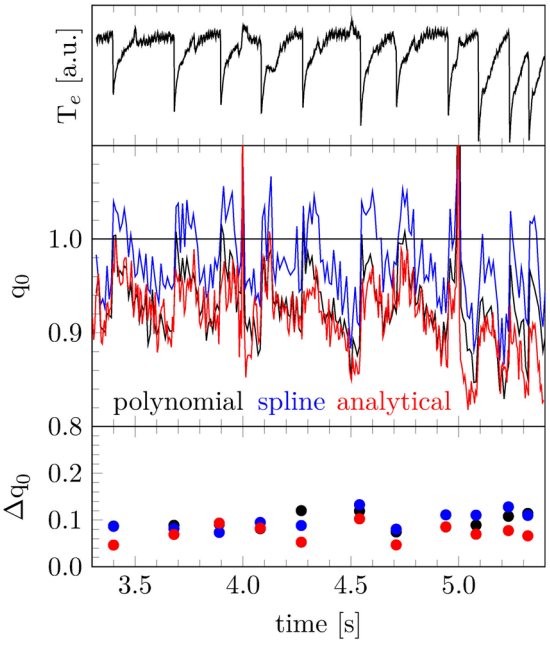

Figure 11. Top: Time evolution of the electron temperature from a central ECE channel. Centre: q_0 determined form EFIT reconstruction and analytical solution. Bottom: Change in q_0 at the sawtooth crash. Note that the q-profile can not be reconstructed during the NBI blips at $t = 3.5, 4.0, 4.5, 5.0$ s.

a suitable discharge with a sawtooth period of $\tau_s \approx 150$ ms –300 ms (see figures 10 and 11) has been identified. The characteristics of the increased sawtooth period are similar to the monster sawteeth reported by Campbell [18], where a stabilisation of the sawteeth by NBI injection was observed. In the analysed discharge the fast particle pressure p_{fast} was estimated from the injected NBI power, acceleration voltage and slowing down time. With a back-of-an-envelope calculation p_{fast} is estimated to account for up to 10% of the total pressure. This non-negligible fast particle pressure may be the reason for the relatively long sawtooth period in this particular discharge. However, the presented method of deducing the

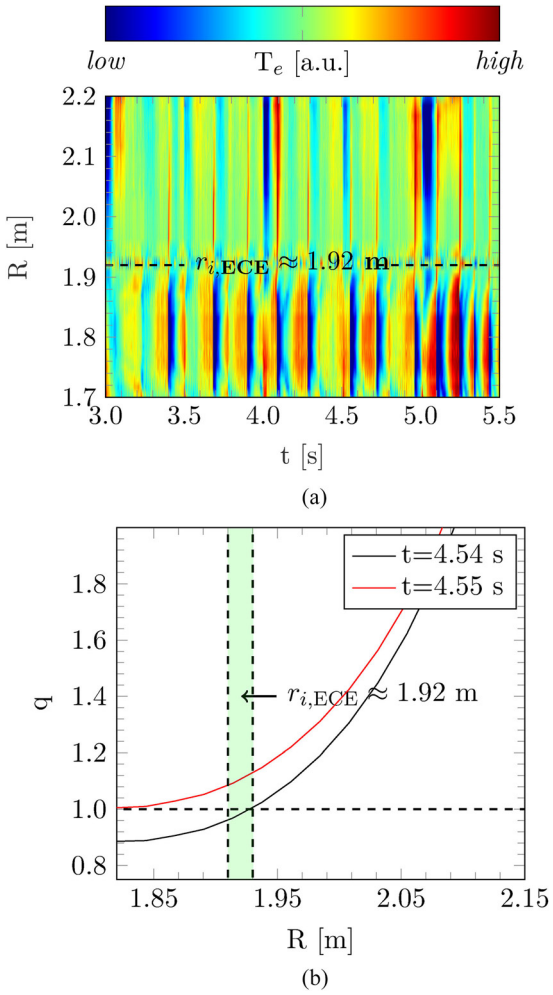

Figure 12. Comparison of the sawtooth inversion radius determined from ECE analysis (*a*) and q-profile reconstruction (*b*). (*a*) Normalized time evolution of the electron temperature profile. The inversion radius has been determined from the graph to $r_{i,ECE} = 1.92$ m, the position at which the the change in temperature at the sawtooth crash inverses. (*b*) Reconstructed q-profile (polynomial method) before and after a sawtooth crash. The green shaded area marks the approximate location of the sawtooth inversion radius determined from (*a*).

q-profile and magnetic axis does not rely on the fast particle content, but only on the total pressure.

In Campbell's analysis the evaluation of the safety factor was limited to magnetic measurements by which q_0 was determined to approximately 0.9–1.0 during the quiescent time.

This can be compared to the reconstructed evolution of safety factor at KSTAR, shown in figure 11, where q_0 has been reconstructed using three different analysis methods: the curves marked as polynomial (—) and spline (—) result from the equilibrium reconstruction using EFIT, where for the first a second order polynomial is used to describe the basis function of the current density profile and for the later three splines have been chosen as basis function. The spline location is chosen at the plasma centre, at the edge and roughly at the location of the sawtooth inversion radius. The remaining parameters have been kept constant during the EFIT analysis. The third curve labelled analytical (—) is the analytical solution of q_0 derived by Petty [19]:

$$\mathrm{q_0} = -\frac{\kappa}{\mathrm{R_0}}\left(\frac{\partial}{\partial R}\tan(\gamma_m)\right)^{-1}\Bigg|_{\mathrm{R=R}_m}. \qquad (1)$$

Here, κ is the plasma elongation, $\mathrm{R_0}$ the major radius and γ_m is the magnetic pitch angle at the magnetic axis R_m. κ has been obtained by reconstructing the plasma equilibrium using EFIT only constrained by magnetic measurements, which is believed to give the most accurate solution for the plasma boundary. For the analytical analysis a three point moving mean filter has been applied to the MSE data and for all three analysis methods the polarimetric data is averaged over 10 ms.

The three solutions follow the evolution of the electron temperature closely, a sharp increase of q_0 can be observed at the time of the sawtooth crash followed by a steady decline until the next expulsion of the plasma core. The polynomial and analytical solutions match well in absolute value, whereas $q_{0,\mathrm{spline}}$ is raised by $\Delta \mathrm{q_0} \approx 0.04$. Independent of the analysis method, q_0 drops well below unity between the sawtooth crashes. However, since the error on q_0 is estimated to be on the order of $\Delta \mathrm{q_0} = 0.1$ no definite conclusion can be drawn whether q_0 stays below unity during the entire sawtooth cycle. It is important to point out that this result appears to be in contradiction with results published earlier at KSTAR [5], where $\mathrm{q_0}$ has been determined to stay above or close to unity by using the analytical solution. Possible explanations for this difference include: (a) a difference in the discharge regime. (b) in reference [5], κ was calculated by KSTAR's real-time version of EFIT, which is considered to be less accurate than the post-shot analysis version. (c) possible the treatment of the radial electric field, which was assumed to be negligible in [5].

As the last analysis step, the location of the sawtooth inversion radius is compared between the reconstructed q-profile and ECE measurements. Figure 12(*a*) shows the time evolution of the normalised temperature profile using KSTAR's ECE system from which the inversion radius is determined to $r_{i,\mathrm{ECE}} = 1.92$ m. Figure 12(*b*) shows the q-profile before and after a sawtooth crash (polynomial basis functions), which is in good agreement with the inversion radius determined by ECE. The analysis shows a broadened safety factor profile, similar to observations by Mc Cormick *et al* at the ASDEX tokamak [20], where sawteeth were stabilised with lower hybrid current drive (LHCD). However, in Mc Cormick's analysis q_0 relaxed to values above unity after the sawtooth crash, whereas our analysis is in agreement with the q_0 evolution at JET's stabilized sawteeth [18]. An important difference between the experiments at KSTAR and JET compared to ASDEX is the amount of non-inductive driven current which was reported to be almost fully non-inductive at ASDEX, but negligible at KSTAR and JET. Dedicated experiments are required to check whether a change in sawtooth behaviour can be observed at KSTAR during non-inductive operation.

5. Conclusion

In conclusion we have shown that with a two-step calibration procedure the MSE diagnostic at KSTAR provides physically sensible magnetic pitch angle measurements with a resolution

of 10 ms and an accuracy of $0.1° - 0.5°$. The diagnostic is now ready for routine operation and has been used to measure the evolution of the central safety factor of a discharge with sawteeth instability with exceptionally long sawtooth periods. The MSE measurements show an increase in q_0 from 0.9 to 1 at the time of the sawtooth crash, where the uncertainty of q_0 is estimated to be $\Delta q_0 \approx 0.1$. This is inline with the reconnection model proposed by Kadomtsev, however it was shown that the analysis is very sensitive to choice of basis functions used to describe the current density. For the future a more in depth analysis of the sawtooth behaviour at KSTAR is required to gain further insight on the evolution of the current density profile. The focus should clearly be on the analysis of multiple shots to get a higher statistical confidence in the result, the analysis of non-stabilized sawteeth as well as the sawteeth behaviour during non-inductive operation to see if a raised q-profile, similar to the results measured at ASDEX is obtained.

Acknowledgment

M.C.C. Messmer would like to thank Dr. Hyun-Seok Kim and Dr. Sang-hee Hahn of NFRI for the many fruitful discussions and support with the equilibrium reconstruction.

This work was supported by the research programs funded by the Ministry of Science and ICT in Korea.

Appendix. Detailed description of the determination of the systematic offset

Section 3.2 briefly described the determination of a systematic offset in the measured polarisation angles. The detailed procedure is described here. As afore mentioned, a reconstruction of the current density profile using the equilibrium solver EFIT constrained by polarisation angle measurements was initially unsuccessful due to non-convergence of EFIT. This has been attributed to an unaccounted systematic offset in the measurement. A channel independent, constant offset is assumed due to the shape of the polarisation angle profiles obtained after the bandpass filter calibration in section 3, which imply physically sensible measurements.

To verify the hypothesis of the systematic offset, the plasma equilibrium of a shot is reconstructed with varying systematic offsets applied to the MSE data. The resulting q-profiles are compared to tearing modes of known mode number and location. The ideal offset is found where the best match is made.

A.1. Tearing mode analysis

Reference values for the by EFIT reconstructed, expected q-profile are obtained by an independent tearing mode (TM) analysis. The MHD mode numbers are determined by analysis of Mirnov Coil (MC) signals and the location of the instability is obtained by cross-correlating electron cyclotron emission (ECE) measurements with the MC data. The result of the analysis is shown in figure A1, where the spectrogram of one of the toroidal MC is plotted, labeled with the determined mode

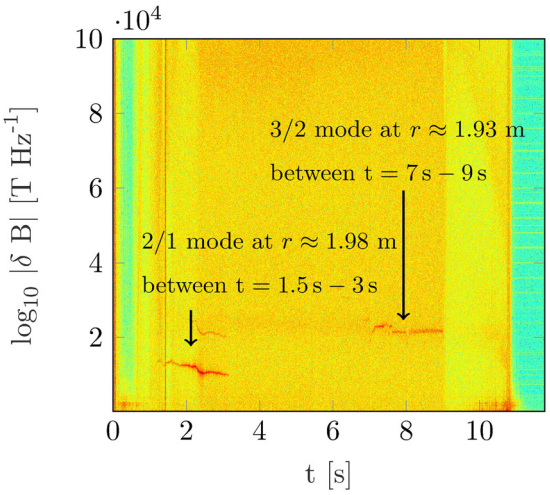

Figure A1. Spectrogram of one of the toroidal MC of shot *#13728*: From Mirnov Coil and ECE analysis a 2/1 mode between 1.5 s–3 s and a 3/2 mode between 7 s–9 s have been determined. The MHD activity was suppressed from 3 s–7 s by ECRH.

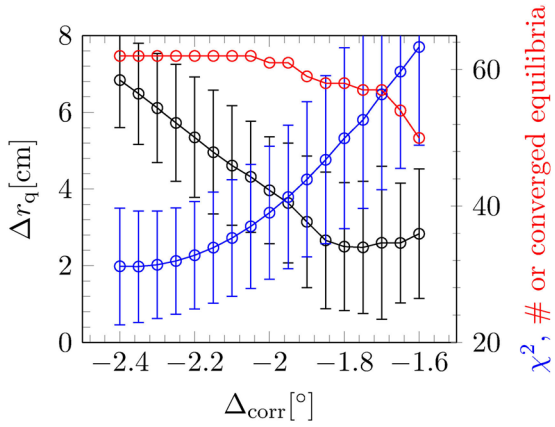

Figure A2. Calibration analysis for shot *#13728*: Difference in boundary Δr_q, χ^2 and the number of time steps for which EFIT was able to converge are plotted over the systematic correction factor Δ_{corr}. The uncertainties are above what one would expect by purely looking at the spread of the data, however they do represent the statistical spread of the data and no systematic error could be determined.

numbers and locations. A 2/1 mode at approximately 1.98 m is present between 1.5 s–3 s and a 3/2 mode at 1.93 m has been observed between 7 s–9 s. In the intermediate time interval the modes were suppressed by ECRH.

A.2. Determination of the systematic offset

To determine the systematic offset in the polarisation angle measurements, a stepwise increasing, channel independent correction factor $\Delta_{corr} \in [-3.8°, +2.4°]$ is added to the measured polarisation angles. For each step in Δ_{corr} the plasma equilibrium is reconstructed and the following quantities are evaluated:

1. The difference Δr_q between the MHD mode location obtained from MC+ECE analysis and the location of the q-surface from the EFIT reconstructed q-profile.

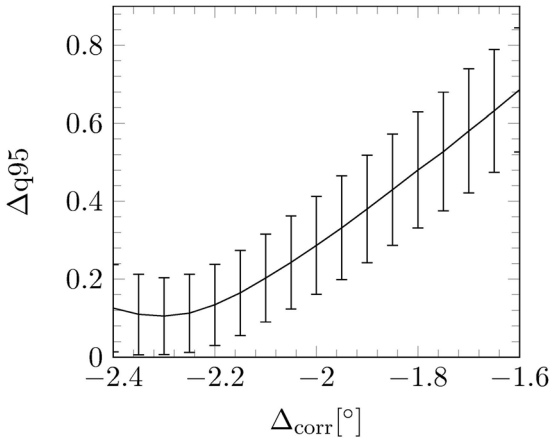

Figure A3. Calibration analysis for shot *#13728*: Difference in Δq_{95} over the systematic correction factor Δ_{corr}. Δq_{95} as a minimum at $\Delta_{corr} \approx -2.3°$.

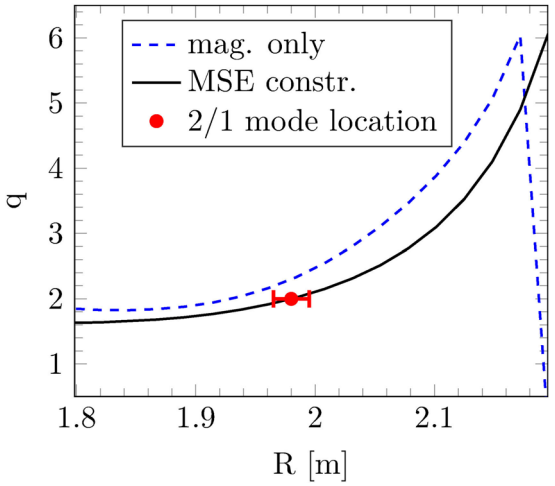

Figure A4. Comparison of reconstructed q-profile for shot *#13728* at $t = 1.9$ s with and without MSE constraint. The indicated location of the 2/1 mode (magenta) is the position determined by MS + ECE diagnostic.

2. The convergence of EFIT, reflected by the fit value χ^2 (lower is better).
3. The number of time steps for which EFIT converged.
4. The value of safety factor at the plasma edge q_{95}, more precisely the difference $\Delta q_{95} = |q_{95,mag} - q_{95,MSE}|$. Here, $q_{95,MSE}$ is the value of q_{95} determined by MSE constrained EFIT and $q_{95,mag}$ the edge safety factor determined by magnetics only EFIT. This is an important benchmark quantity as magnetics only EFIT is expected to give accurate results for the plasma edge.

For the analysis a combined total of 61 time points for the 2/1 and 3/2 TM are evaluated, where for each time the measurement signals are averaged over 50ms. For the final evaluation of the four criteria listed above, the 61 individual time steps are averaged for each correction factor.

The analysis has been performed for correction factors ranging from $\Delta_{corr} \in [+2.4°, -3.8°]$, however only the results of the analysis from $-2.4°$ to $-1.6°$ are discussed as it has been found to be the relevant interval. Figure A2 shows Δr_q

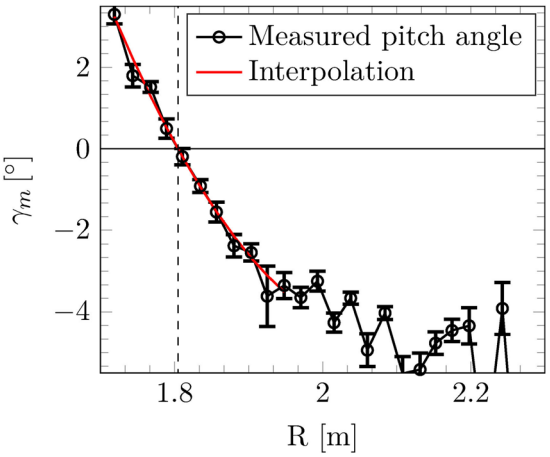

Figure A5. Determination of the magnetic axis. The 10 innermost channels are interpolated by a third order polynomial fit from which the magnetic axis can be derived by calculating the intersection of the fit with the x-axis, indicated by the dashed line.

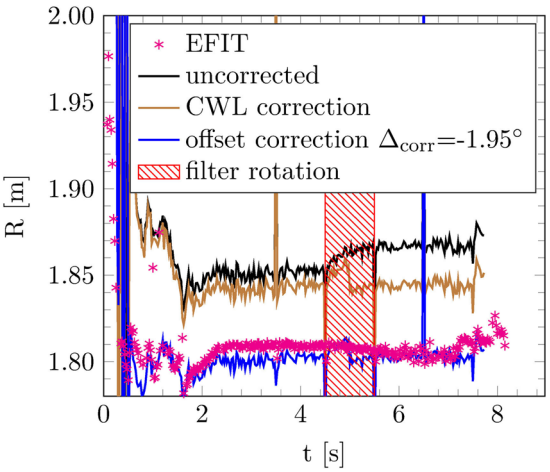

Figure A6. Comparison of the magnetic axis for shot *#13691* between MSE analysis and the axis location reconstructed from magnetics only EFIT. The MSE measurements are corrected to account for the incorrectly set CWL of the bandpass filters and the systematic offset.

as well as χ^2 and the number of time steps for which EFIT converged over Δ_{corr}; Δq_{95} over $\Delta_{corr}$is plotted in figure A3.

The difference in the tearing mode location Δr_q has a minimum of $\Delta r_{q,min} \approx 2.7$ cm at $\Delta_{corr} = -1.85°$, showing good agreement between MSE EFIT and the TM location determined via MC+ECE. However, Δq_{95} has a minimum at $\Delta_{corr} = -2.3°$, which is inline with the observation that χ^2 decreases for smaller values of Δ_{corr}. For offsets greater than $-1.6°$, χ^2 rises rapidly and EFIT is unable to find a converging solution.

From the analysis no conclusive ideal offset can be determined and thus a compromise solution was made and $\Delta_{corr,opt} = -1.95°$ has been selected as the ideal correction factor. With this, Δr_q is close to its minimum, the difference in Δq_{95} is acceptable low and EFIT shows good convergence.

Applying the determined optimal correction factor to the recorded polarisation angles, figure A4 shows the comparison of the MSE constraint and magnetics only reconstructed

q-profile for $t = 1.9$ s of the calibration shot. The location of the 2/1 TM is in good agreement with the MSE EFIT reconstructed q-profile.

To further verify that the chosen offset does indeed provide sensible results, the now fully calibrated system is tested by comparing the location of the magnetic axis calculated from the measured polarisation angles against the axis location determined from magnetic probes.

A.3. Independent verification of Δ_{Off} and Δ_{corr}

For an independent test of the filter rotation calibration and the determined systematic offset in the polarisation angles, the position of the magnetic axis is verified by comparing the location calculated from the polarisation angle profiles against magnetics only EFIT. For the comparison, one of the MSE calibration shots described in section 2 is evaluated. For this L-mode discharge magnetics only EFIT is expected to provide accurate results. The position of the magnetic axis from the MSE data is obtained by interpolation the zero crossing of a third order polynomial fit to the first 10 channels neighbouring the magnetic axis as shown in figure A5. A third order fit was chosen as it resembles the shape of the measured profile, although a second order fit provides similar results.

Figure A6 compares of the time evolution of the magnetic axis with the two corrections applied to the MSE data: —— marks the time evolution obtained from the uncorrected pitch angles. The measured data was first corrected to account for the incorrect filter rotation (described in section 3.1), resulting in the —— graph. Secondly, the pitch angles are corrected to account for the systematic $-1.95°$ offset, resulting in the —— graph. This is in excellent agreement with the EFIT result $***$, giving confidence in both filter calibration and the determined systematic offset.

ORCID iDs

M.C.C. Messmer https://orcid.org/0000-0001-8102-0668

References

[1] Levinton F.M., Fonck R.J., Gammel G.M., Kaita R., Kugel H.W., Powell E.T. and Roberts D.W. 1989 Magnetic field pitch-angle measurements in the PBX-M Tokamak using the motional Stark effect *Phys. Rev. Lett.* **63** 2060–3

[2] Lao L.L., Ferron J.R., Groebner R.J., Howl W., John H.S., Strait E.J. and Taylor T.S. 1990 Equilibrium analysis of current profiles in tokamaks *Nucl. Fusion* **30** 1035

[3] Oh Y.-K. *et al* 2016 Overview of the KSTAR research in support of ITER and DEMO *Preprint: 2016 IAEA Fusion Energy Conf. Proc. (Kyoto)* OV/2–4

[4] Ko J., Chung J. and Messmer M. 2016 Diagnostic development for current density profile control at KSTAR *Fusion Eng. Des.* **109-111** 742–6

[5] Ko J. 2016 Sensitivity of magnetic field-line pitch angle measurements to sawtooth events in tokamaks *Rev. Sci. Instrum.* **87** 11E541

[6] Chung J., Ko J., De Bock M.F.M. and Jaspers R.J.E. 2014 Instrumentation for a multichord motional Stark effect diagnostic in KSTAR *Rev. Sci. Instrum.* **85** 827

[7] Chung J., Ko J., Wi H., Messmer M., Schenkelaars S., Scheffer M. and Jaspers R.J.E. 2016 Initial operation of a newly developed multichord motional Stark effect diagnostic in KSTAR *Rev. Sci. Instrum.* **87** 503

[8] De Bock M.F.M., Conway N.J., Walsh M.J., Carolan P.G. and Hawkes N.C. 2008 *Ab initio* modeling of the motional Stark effect on MAST *Rev. Sci. Instrum.* **79** 10F524

[9] von Goeler S., Stodiek W. and Sauthoff N. 1974 Studies of internal disruptions and $m = 1$ oscillations in Tokamak discharges with soft-x-ray techniques *Phys. Rev. Lett.* **33** 1201–3

[10] Kadomtsev B.B. 1975 Disruptive instability in Tokamaks *Sov. J. Plasma Phys.* **1** 389

[11] Wesson J.A. 1986 Sawtooth oscillations *Plasma Phys. Control. Fusion* **28** 243–8

[12] Soltwisch H. 1988 Measurement of current-density changes during sawtooth activity in a tokamak by far-infrared polarimetry (invited) *Rev. Sci. Instrum.* **59** 1599–604

[13] Yamada M., Levinton F.M., Pomphrey N., Budny R., Manickam J. and Nagayama Y. 1994 Investigation of magnetic reconnection during a sawtooth crash in a high-temperature tokamak plasma *Phys. Plasmas* **1** 3269–76

[14] O'Rourke J. 1991 The change in the safety factor profile at a sawtooth collapse *Plasma Phys. Control. Fusion* **33** 289–96

[15] Koslowski H.R. 2005 Overview of current density measurements and sawtooth studies on TEXTOR *Fusion Sci. Technol.* **47** 260–5

[16] Wróblewski D. and Lao L.L. 1991 Determination of the safety factor in sawtoothing discharges in DIII-D *Phys. Fluids B Plasma Phys.* **3** 2877–81

[17] Wróblewski D. and Lao L.L. 1992 Polarimetry of motional Stark effect and determination of current profiles in DIII-D (invited) *Rev. Sci. Instrum.* **63** 5140–7

[18] Campbell D.J. *et al* 1988 Stabilization of sawteeth with additional heating in the JET tokamak *Phys. Rev. Lett.* **60** 2148–51

[19] Petty C.C., Politzer P.A. and Lin-Liu Y.R. 2005 Direct measurement of neoclassical currents using motional Stark effect polarimetry *Plasma Phys. Control. Fusion* **47** 1077–100

[20] McCormick K. *et al* 1987 Temporal behavior of the plasma current distribution in the ASDEX tokamak during lower-hybrid current drive *Phys. Rev. Lett.* **58** 491–4